2016

Optimisation of Anodic Oxidation of Aluminium for Enhanced Adhesion and Corrosion Properties of Sol-gel Coatings.

Michael Whelan
Technological University Dublin, michael.g.whelan@tudublin.ie

Tobin Edmond
University of Limerick, edmond.tobin@ul.ie

John Cassidy
Technological University Dublin, john.cassidy@tudublin.ie

J. Colreavy
Centre for Research on Engineering Surface Technology (CREST), FOCAS Institute, Technological University Dublin

Brendan Duffy
Technological University Dublin, brendan.duffy@tudublin.ie

Recommended Citation

Whelan, M. et al. (2016) Optimisation of Anodic Oxidation of Aluminium for Enhanced Adhesion and Corrosion Properties of Sol-gel Coatings, *Journal of The Electrochemical Society,* 163 (5) C1-C8 (2016) DOI : 10.1149/2.0741605jes

Journal of The Electrochemical Society, **163** (5) C1-C8 (2016)
0013-4651/2016/163(5)/C1/8/$33.00 © The Electrochemical Society

Optimisation of Anodic Oxidation of Aluminium for Enhanced Adhesion and Corrosion Properties of Sol-Gel Coatings

M. Whelan,[a,z] Edmond Tobin,[b] J. Cassidy,[c] and B. Duffy[a]

[a]*Centre for Research in Engineering Surface Technology, Focas Institute, Dublin Institute of Technology, Dublin 8, Ireland*
[b]*Department of Mechanical, Aeronautical and Biomedical Engineering, University of Limerick, Limerick, Ireland*
[c]*Department of Chemical and Pharmaceutical Science, Dublin Institute of Technology, Dublin 8, Ireland*

The anodising process for clad and bare AA2024-T3 has been optimised as a surface preparation technique prior to sol-gel coating deposition. The combination of anodised aluminum surfaces and organically functionalised sol-gel chemistry have been investigated to impart elevated corrosion resistance and increased mechanical properties to the aluminum metal. A duplex anodising process has been developed to utilise the natural corrosion resistance properties of sulphuric acid anodising with the adhesion and hosting properties of phosphoric acid anodising. The novel anodising process and sol-gel sealed surfaces have been characterized using field emission scanning electron microscopy, energy dispersive X-ray spectroscopy. Performance of the sol-gel treated anodic layers is evaluated by neutral salt spray testing, electrochemical impedance spectroscopy and rain erosion testing.

Manuscript submitted November 30, 2015; revised manuscript received January 22, 2016. Published 00 0, 2016.

Aluminium is used extensively for lightweight structures such as automotive and aerospace components where the combination of strength and corrosion resistance is essential. Aluminium owes its inherent corrosion resistance to a naturally occurring passive oxide which forms on the metal when exposed to the atmosphere.[1] This oxide is nanometre in thickness which limits the metals performance against extreme mechanical and chemical attack.[2]

Anodising is a process which increases the thickness of the aluminum oxide through an electrochemical reaction in acidic electrolytes such as sulphuric, phosphoric or oxalic acids.[1] The features and properties of the anodic oxides produced are dependent on many parameters including the aluminum alloy, electrolyte type and anodising conditions (e.g. temperature and current density). The process is commonly used to increase corrosion resistance and adhesion properties of the aluminum surface for a variety of applications.

The anodised aluminum oxide layer is nanoporous in structure with a self assembled, hexagonal array of pores extending from the surface of the oxide to a thin barrier layer at the metal oxide interface. The oxide growth and nanopore formation mechanism is a result of flow of anodic alumina in the barrier layer region due to the combination of growth stresses and field assisted plasticity.[3–5] The stresses that drive the flow of material are due to electrostriction of the oxide layer which is plasticised under the electric field.[4–6] The flow of material proceeds from the barrier layer into the pore walls forming Al_2O_3 columns in a self assembled structure.

For anti-corrosion applications sulphuric acid anodising (SAA) is most commonly employed.[1] A significant advantage of SAA anodic layers is the ability of the pores to close by surface hydration resulting in elevated barrier properties. Hydration on the SAA surface proceeds rapidly after anodising and can be accelerated by hydrothermal treatment to achieve increased corrosion protection while also entrapping any applied inhibitors of dyes.[7] Both natural and hydrothermal induced hydration results in pore blocking near the surface of the anodised layer. Hydration continues naturally over time as the pore closing effects move down the pore channel toward the metal surface.[8] This continued hydration termed "auto-sealing" results in an increase in the barrier properties of the anodic layers even during exposure to aggressive environments.[9–11] Such as feature is responsible for the excellent long term and accelerated corrosion resistance of sulphuric acid anodised layers on copper free wrought alloys.

In the case of copper containing alloys, the protection properties afforded from anodic layers by sulphuric acid anodising is reduced by the inclusion of Cu rich intermetallics in the metal as well as Cu ions within the oxide network.[12] The presence of Cu as well as the random orientation of the pores leads to difficulties with hydration sealing.[13] To improve the protection on copper containing alloys, novel anodising processes have been developed including boric-sulphuric (BSAA) and tartaric-sulphuric (TSAA) acid anodising for corrosion and adhesive bonding applications. TSAA in particular offers significant advantages over thin film SAA due to the Cu chelating ability of the tartrate ions which increases the barrier properties of the formed layers.[14]

Despite the development of novel anodising treatments for copper rich aluminum alloys, the corrosion protection afforded by the anodic layers is limited. To fully protect the aluminum metal the development of novel sealing technologies is required. Sol-gel materials have been extensively studied for corrosion control replacements for Cr(VI) based conversion coatings and are currently being investigated as potential sealing technologies for anodised aluminum.[9] The sol–gel process can be used to form nanostructured inorganic films (typically 200 nm to 10 μm in overall thickness) that can be tailored to be more resistant than metals to oxidation, corrosion, erosion and wear while also possessing good thermal and electrical properties.[15–17] The chemistry of the sol–gel process is well known[18–20] with excellent reviews[21–23] and books[24] available. The most common sol–gel materials used as coatings are based on organically modified silicates (ormosils), which are formed by the hydrolysis and condensation of alkoxide precursors.[25]

Sol-gel coatings can potentially be tailored to act as sealing agents for anodised aluminum. There are however some inherent problems associated with the combination of sol-gel chemistry and sulphuric acid anodised aluminum layers. Migration of sol-gel materials into the aluminum oxide pores can be limited.[26] Furthermore the presence of sol-gel material in the pores of the anodic layers has shown to postpone or fully inhibit the natural hydration of the anodic layers. For the deposition of sol-gel materials on anodic layers it is essential to achieve encapsulation into the porous oxide matrix. This ensures that the hardness and abrasion resistance properties of the anodised surface are afforded to the sol-gel network. It has been reported that sol-gel coatings applied on TSAA anodised aluminum delaminate from the oxide surface after extended corrosion testing.[27] If encapsulation is achieved it is critical that the presence of the sol-gel sealer does not affect the hydration and auto-sealing mechanisms of the anodic layers.

For adhesion applications where increased corrosion resistance is not a factor, phosphoric acid anodising (PAA) is also a commonly utilised.[1] The large pore diameters as well as the slow hydration rate of the PAA oxide makes it ideal as an intermediate treatment between the aluminum metal and any applied coatings or adhesives. Unlike the SAA process, PAA treatment imparts limited additional protection to the aluminum surface as hydration induced sealing is not possible, which limits its use in anti-corrosion applications. Recently PAA has been utilised as a successful encapsulation matrix for sol-gel coatings[9] however protection properties are limited due to the absence

[z]E-mail: michael.g.whelan@dit.ie

of significant oxide hydration. In order to achieve both encapsulation of sol-gel materials and unaltered surface hydration, a duplex anodic structure is required. A duplex anodic layer consists of an anodic layer formed from a double anodising process conducted in two different electrolytes. Duplex structures have previously been reported as a result of electro-deoxidising and anodising.[28]

To optimise the surface preparation of the aluminum surface, a novel anodising process was developed to produce duplex anodic structures on the surface of aluminum alloys. The process was developed to overcome the limitations between forming voltage for the PAA and SAA treatments so that the parameters of each step could be chosen independently. In this way the PAA layer can be tailored to achieve optimum sol-gel encapsulation while the SAA can be used without sol-gel penetration into the pores therefore not affecting the oxide layer hydration. The duplex anodic structure has been utilised for sol-gel deposition however it can be used for any applications requiring combined corrosion resistance of SAA layers with the adhesion properties of PAA.

Experimental

Sol-gel synthesis.—Two sol-gel coatings were synthesised and used as sealers for the anodic layers.

Phenyl functionalised sol-gel.—The silane precursor phenyltriethoxysilane (PhTEOS) (98%) was purchased from VWR International Ltd (Irl). Hydrolysis was conducted under acidic conditions by adding 5.2 ml of 0.04 M HNO_3 to 50.6 ml of silane precursor. 30.6 ml of absolute ethanol was immediately added to the mixture and left to stir for 45 minutes. 13.6 ml of de-ionised water was then added dropwise and the solution was left to stir for 24 h before use. The final molar ratio for the formulation was Silane: Ethanol: Water - 1:2.5:3.5.

Silane-zirconium hybrid sol-gel.—A silane-zirconium sol-gel formulation (Si-Zr) developed previously[17,29] was also utilised for this work. The silane precursor, 3-(trimethoxysilyl) propylmethacrylate (MAPTMS) (Sigma Aldrich, Irl, Assay (99%) was pre-hydrolysed using 0.01 N HNO_3 for 45 min (solution A). Simultaneously, zirconium (IV) n-propoxide (TPOZ) (Sigma Aldrich, Ireland, Assay ∼70% in propanol) was chelated using methacrylic acid (MAAH) (Sigma Aldrich), at a 1:1 molar ratio for 45 minutes (solution B) to form a zirconium complex. Solution A was slowly added to solution B over ten minutes. Following another 45 min, water (pH 7) was added to this mixture. The molar ratio of Si/Zr in the final sol is 4:1 and Si/H_20 is 1:2. After 24 hours of stirring 3,6-Di-2-pyridyl-1,2,4,5-tetrazine (DPTZ) was added as a corrosion inhibitor at a concentration of 0.3% w/v of MAPTMS precursor.

Pre-treatment and anodising.—Unclad AA2024-T3 (Si 0.5%, Fe 0.5%, Cu 0.8-4.9%, Mg 1.2-1.8%, Mn 0.3-0.9%, Cr 0.1%, Zn 0.25%, Ti 0.15% other 0.15%, Al remainder) aluminum panels (150 mm × 100 mm × 0.6 mm) were sourced from Amari (Irl). The panels were degreased in acetone, etched in Novaclean 104 for 45 secs, rinsed and etched in Novox 302 for 90 seconds. Novaclean and Novox were purchased from Henkel (Ger). Acetone, NaOH, HNO_3, H_2SO_4 and H_3PO_4 were purchased from Sigma Aldrich IRL.

AA2024 clad panels with 40 μm of AA1230 (Si 0.2%, Fe 0.5%, Cu 0.03%, Zn 0.03%, Mn 0.03%, Mg 0.005%, Al remainder) were degreased in acetone, etched in 10% NaOH at 40°C for 50 seconds and rinsed in de-ionised water. The panels were then treated in 50% HNO_3 at room temperature for 90 seconds to remove any intermetallics from the surface prior to anodising.

Anodising solutions were prepared by diluting 98% H_2SO_4 w/v and 95% H_3PO_4 in deionised water to a concentration of 25% w/v and 10% w/v respectively. Three anodising procedures were conducted as follows:

1. Phosphoric Acid Anodising (PAA) – 60 min phosphoric acid anodising at constant 40 V.
2. Sulphuric Acid Anodising (SAA) - 20 min sulphuric acid anodising at 1.5 A/dm^2 of aluminum surface area.
3. Duplex Anodising (DA) - PAA process was conducted as per procedure 1). At the end of the PAA cycle the anodising current was immediately reduced to half of its steady state value. As a result the anodising potential gradually decreased. Once the anodising voltage decreased to 10 V the power was turned off. The surfaces were then rinsed in de-ionised water for 10 min to remove any residual electrolyte from the pores. The parts were then immersed in the sulphuric acid electrolyte. AA2024-T3 and Clad AA2024-T3 were anodised for 5 and 2 min respectively at 1.5 A/dm^2 of aluminum surface area.

All anodised samples were rinsed for 20 min in de-ionised water and air dried prior to sol-gel application and testing.

Sealing in sol gel.—For the PAA and SAA surfaces the sol-gel solution was applied immediately after rinsing and drying by a dip coating process. The DA surface was hydrothermally sealed in de-ionised water at 95°C ± 5 for 5 min prior to sol-gel dip coating. In all cases the dip cycle consisted of a 20 minute immersion step in the sol-gel solution following withdrawal at a rate of 10 mm.min^{-1}. The panels were then cured in an oven at 110°C for 16 hours. Hydrothermally sealed (HTS) equivalents of the DA and SAA layers were also produced for comparison.

Electron microscopy.—The anodised films were analyzed by electron microscopy using a Hitachi SU 70 Field Emission Scanning Electron Microscope (FESEM). Anodic film cross sections were prepared by bending the aluminum sample over 180° to induce micro-cracks in the oxide layer. The cross section of the crack face exhibits the pore structure of the anodic alumina for imaging at 1.5 – 4 keV. For imaging purposes the samples were sputter coated with a 4 nm layer of Pt/Pd using a Cressington 208HR sputter coater.

Dot Map energy dispersive X-ray spectroscopy was conducted using an Oxford instruments INCA X-MAX Energy dispersive X-ray spectrometer attached to the FESEM. Cross sections were prepared by mounting samples in epoxy resin then grinding and polishing to a mirror finish using progressive grades of carbide paper and polished to a 1 μm finish with a diamond solution. The polished cross sections were coated with 5 nm of carbon using a Cresssington 208C Carbon evaporation coating unit. The Si based sol-gels can be identified by analysing the Si species overlapping with the oxide layer species such as O, P and S.

Electrochemical impedance spectroscopy.—Electrochemical Impedance Spectroscopy (EIS) was conducted on the anodised and sealed AA2024-T3. EIS was carried out using a Solartron SI 1287/1255B system comprising of a frequency analyser and potentiostat operated by CorrView and Z Plot software. A 3.5% NaCl solution was used as the exposure electrolyte and the area of the surface exposed was 4.9 cm^2. A single area of each system was exposed and evaluated. All measurements were made at the open circuit potential (E_{oc}) with an applied 10 mV sinusoidal perturbation in the frequency range 1×10^6 to 1×10^{-1} Hz (10 points per decade). It was found that frequencies lower than this range produced data points with significant noise. Before measurements were taken the open circuit potential was allowed to stabilise to maximum perturbation of 5 mV. Prior to each experiment a calibrated dummy cell was used to ensure the correct measurement of the system. A calibrated reference electrode, checked against an unused control electrode, was used for each experiment.

Neutral salt spray.—Corrosion resistance testing was conducted in a neutral salt spray environment according to BS EN ISO 9227:2006 with the back and sides of each panel protected with an impermeable electrically insulating tape. The test conditions consisted of a neutral salt fog atmosphere generated from 5 wt% aqueous NaCl solution at 35 ± 1°C. The panels were placed at an angle of 20° (±5) from the vertical to allow the salt spray to settle on the test face. The panels

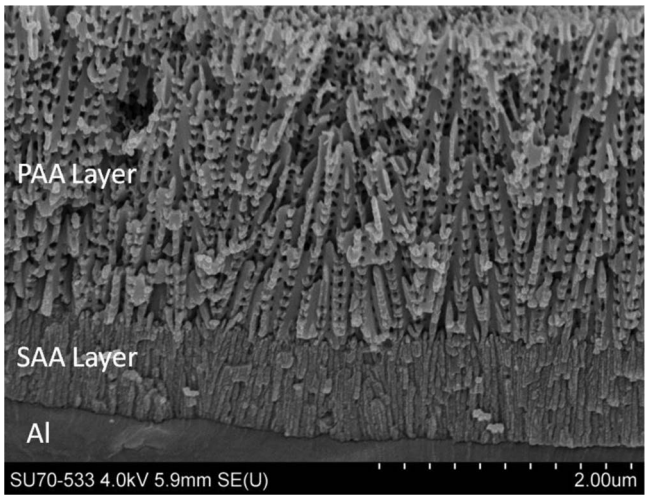

Figure 1. Duplex anodic layer formed on clad AA2024-T3.

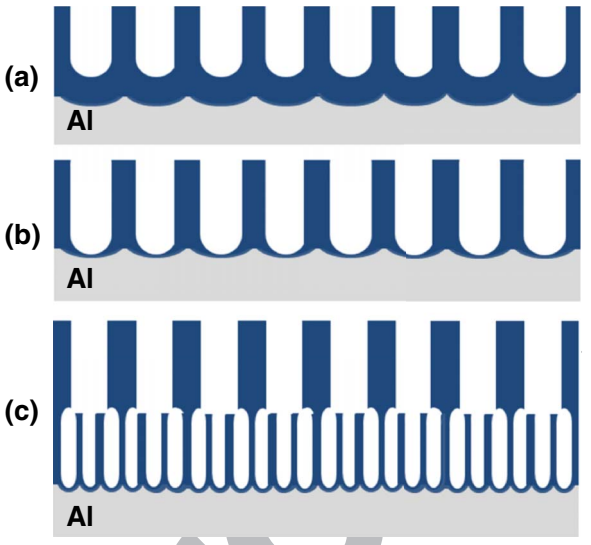

Figure 2. Anodic layer structural change during the duplex anodising cycle.

were exposed to the corrosive conditions for up to 3500 h. A corrosion rating was assigned after each inspection based on the grid method specified in BS EN ISO 12373-19:2001.

Rain erosion.—To simulate the effect of rain erosion on the anodised and sol-gel sealed surface, a Whirling Arm Rain Erosion test Rig (WARER) was used. Circular test samples were produced from the anodised and sol-gel treated samples by punch and die. The initial sample mass was recorded. Mass measurements were repeated 3 times and taken using an Ohaus Explorer analytical balance with an accuracy of 0.1 mg. Inspection was also carried out for scratches and surface imperfections before testing. An individual test sample was then mounted at the end of the whirling arm. Tests were carried out at 178 ms^{-1} and weight loss was recorded at four test durations; 15, 30, 45, and 60 min. The total test duration is based on the length of time the droplet system is active. The rainfall rate was 25 mm/h and was monitored by a flowmeter. A cooling system was used to keep the ambient temperature constant during testing. After each test, the coupons were dried with compressed air and the mass recorded again.

Results and Discussion

Anodic layer formation.—SAA treatment of 2024-T3 and clad 2024-T3 alloys have been studied in many publications and the structures and anti-corrosion properties are well documented.[10,13,14,30–32] DA layers have also been previously reported, however the research to date is limited and the process has not been optimised for sol-gel deposition. The current process produces duplex layers of unique structure as seen in the electron micrograph in Figure 1.

The duplex structure consists of a SAA layer approximately 1 μm in thickness next to the aluminum base metal. This layer exhibits all the natural properties of conventional sulphuric acid anodising such as a small pore diameter as well as surface hydration and auto-sealing. Attached to the surface of the SAA is approximately 2 μm of oxide produced from the PAA process. The oxide exhibits a large pore diameter with a high level of interporosity. This interconnectivity between pores allows better penetration of liquids into the oxide network as the pressure increase within the pores due to the impinging liquid is easily dissipated.

Conventionally the forming voltage of the PAA process is larger than the SAA process. PAA can be conducted up to 200 V while SAA processes generally do not exceed 25 V.[1] The predominant structural effect of the forming voltage is the relative barrier layer thickness with nano-layers formed at approximately 1 nm/V.[1] The barrier layer has been shown to be a significant feature in the electrochemical response of anodised layers.[33] Due to this difference in forming voltage and subsequent barrier layer thickness, burning and rapid dissolution of the metal can occur during the SAA cycle due to the insulating effect of the previously formed PAA layer. The critical requirement for the formation of DA layer without burning of the aluminum surfaces is the reduction of the barrier layer thickness of the PAA layer prior to the SAA anodising.

After conducting the initial PAA process a porous layer with a relatively thick barrier layer is formed, Figure 2a. The barrier layer formed at the base of the pores is approximately 40 nm in thickness as measured by SEM analysis. It is known that the charge transfer across the barrier is due to ionic conduction of the anodising electrolyte ions as well as Al^{3+} and O^{2-} ions.[34,35] If the barrier layer thickness is not decreased prior to the SAA process, the application of the second lower steady state anodising potential is not sufficient to allow ionic transfer across the barrier layer. Rather than distributing uniformly across the metal surface, the current will conduct through the point of least resistance. It was found that the process of in-situ electrochemical thinning of the barrier layer (Figure 2b) prior to the second anodising process is critical to prevent burning and dissolution of the metal surface due to large build up of current density at weak spots in the first anodic layer.

Barrier layer thinning (BLT) utilises the self regulating nature of the anodising process.[36] By rapidly limiting the current at the end of the PAA process to half of the steady state anodising current, the voltage will gradually decrease from the set 40 V to a lower value. During this decrease in voltage, the self regulating characteristic of the anodising process results in a corresponding thinning of the barrier layer Figure 2b. Once a second steady state anodising voltage is reached, the anodising current can again be halved which results in a further voltage drop and continued barrier layer thinning. This step can be further repeated and by sequentially limiting the current in this way a final steady state voltage of the first anodising process can be lowered below the initial anodising voltage of the second anodising process. The results of a BLT process to 10 V and 2 V can be seen in FESEM images in Figure 3. By lowering the forming voltage to 2 V it can be seen that the barrier layer is almost completely removed. Complete removal of the barrier may however compromise the interfacial adhesion between the anodised layers. Barrier layer thinning to a forming voltage of 10 V is sufficient to allow the second anodising process to proceed and in the present study a single current limiting step was required.

Once the BLT PAA anodised aluminum is immersed in the SAA electrolyte and a potential above 10 V is applied, ionic conduction across the barrier layer will occur. This results in a thickening of the barrier layer and SAA layer pore nucleation initiates. The SAA layer growth then proceeds uninhibited, Figure 2c. The use of an

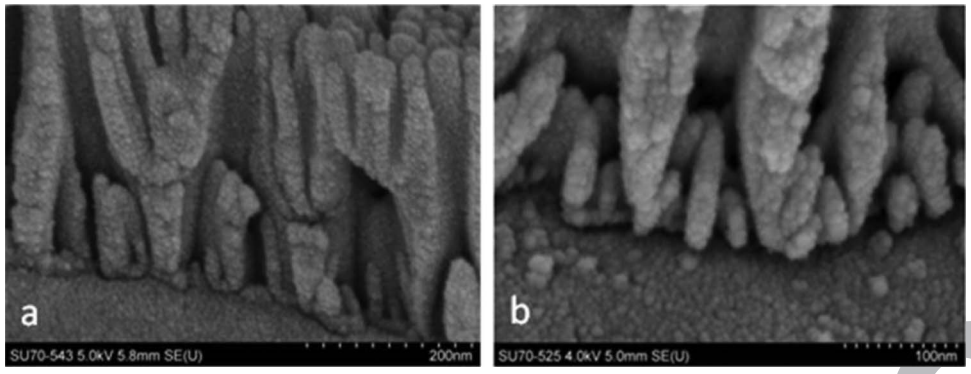

Figure 3. Effect of barrier layer thinning to 10 V (left) and 2 V (right).

intermediate BLT step between the first and second anodising processes allows the parameters for each treatment to be chosen independently. This allows a great deal of flexibility in the layer thickness, pore features and chemical nature of the possible duplex structures that can be formed.

Sol-gel penetration.—There are many factors that can determine if the sol-gel treatment penetrates the porous anodic layers. PAA layers offer the best possibility of penetration due to the large pore diameter, however if the particle size is sufficiently small the sol-gel colloids can also migrate into the SAA layers. In order to determine the penetration properties of the sol-gel on each anodic finish, EDX dot map analysis was used to plot the Si and Al distributions. Figure 4 exhibits the dot maps for the PhTEOS and Si-Zr sol-gel sealed SAA, PAA and DA films on unclad AA2024. The individual layer thicknesses differ from Figure 1, as the alloy is unclad AA2024 as opposed to the clad version in Figure 1.

The PhTEOS exhibits penetration into all surfaces and previous research has shown that the particle size is sufficiently small to allow penetration.[9] On the SAA layer, which contains the smallest pore diameter, it is clear that the PhTEOS sealer has significant penetration into the oxide with Si intensity deteriorating rapidly at approximately 75% of the oxide thickness. The PAA is known to act as an excellent host for sol-gel materials[9] and penetration can be seen again throughout the layer. For the DA layer penetration occurs in the PAA upper layer without evidence of any migration into the SAA base layer probably due to the forced hydration and pore closing between the PAA and SAA layers. In the case of the Si-Zr sol-gel, limited penetration into SAA network occurs. A surface coating only can be distinguished from Figure 4. Similarly to the PhTEOS, the Si-Zr sol-gel penetrates the PAA networks of both the single and duplex anodised layers.

Electrochemical impedance spectroscopy.—EIS analysis was conducted on the un-clad 2024-T3 as the electrochemical response is from the copper rich base metal which is more susceptible to corrosion than the clad material.

The impedance and phase shift spectra for the SAA anodisation with sealers, HTS, PhTEOS and Si-Zr, can be seen in Figure 5. The HTS sealed SAA layer exhibits a characteristic single time constant response. Limited hydration sealing of the pores is detected which is consistent with previous work.[9] Both sol-gel sealers display increased impedance values, for all frequencies, indicating increased barrier properties of the sol-gel sealers compared to the HTS equivalent. The SAA PhTEOS system displayed a single time constant response indicating that the contributions from the sol-gel sealer and the barrier layer cannot be distinguished. From the EDX analysis it is known that

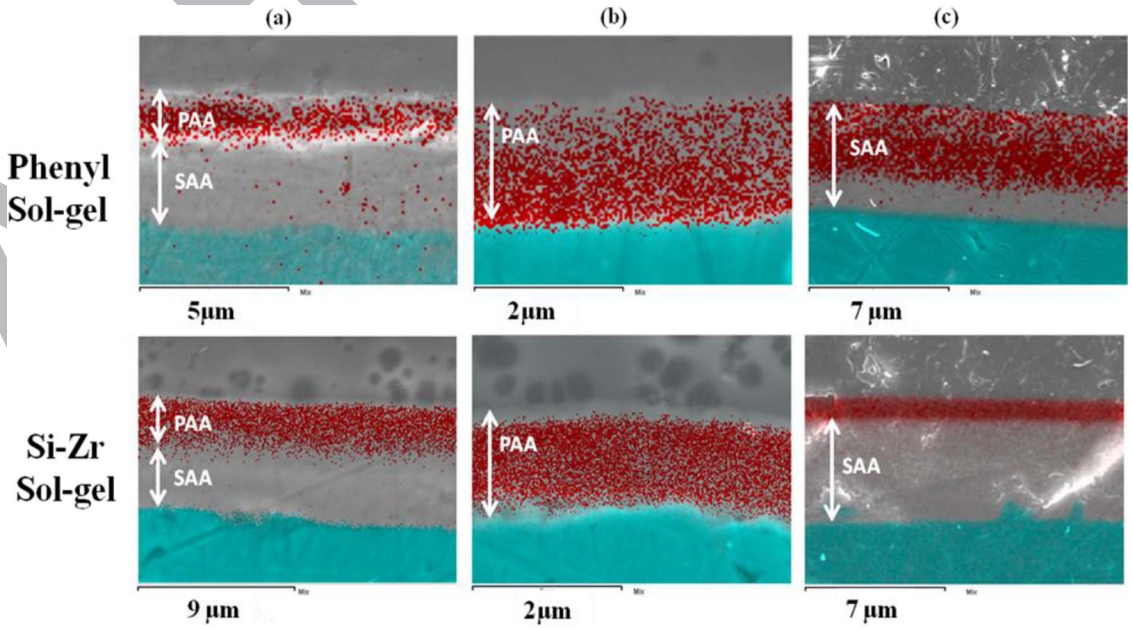

Figure 4. Pore penetration of sol-gel materials (Si (red dots) and Al (blue dots)) into anodised layers on AA2024-T3 (a) DA layer, (b) PAA layer and (c) SAA layer.

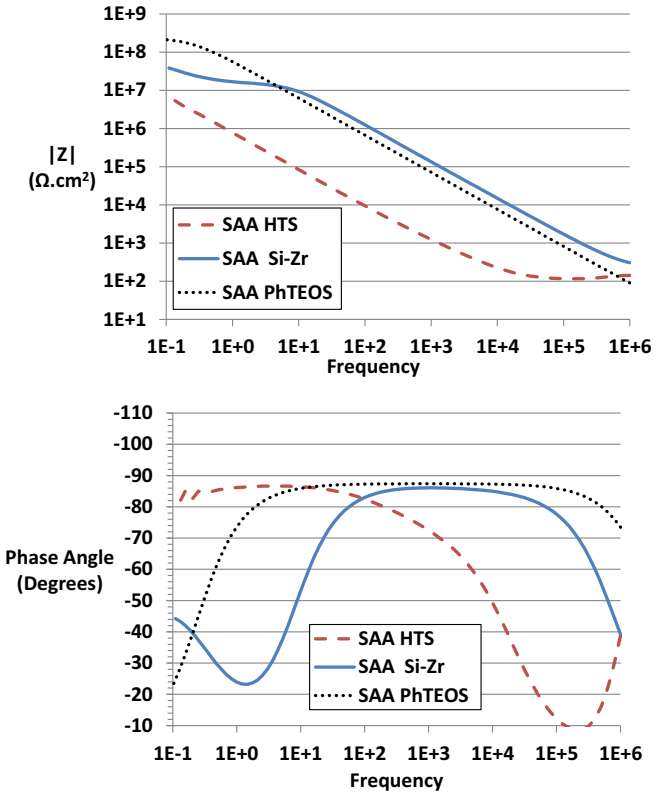

Figure 5. Impedance (top) and phase plot (bottom) for SAA sealed samples.

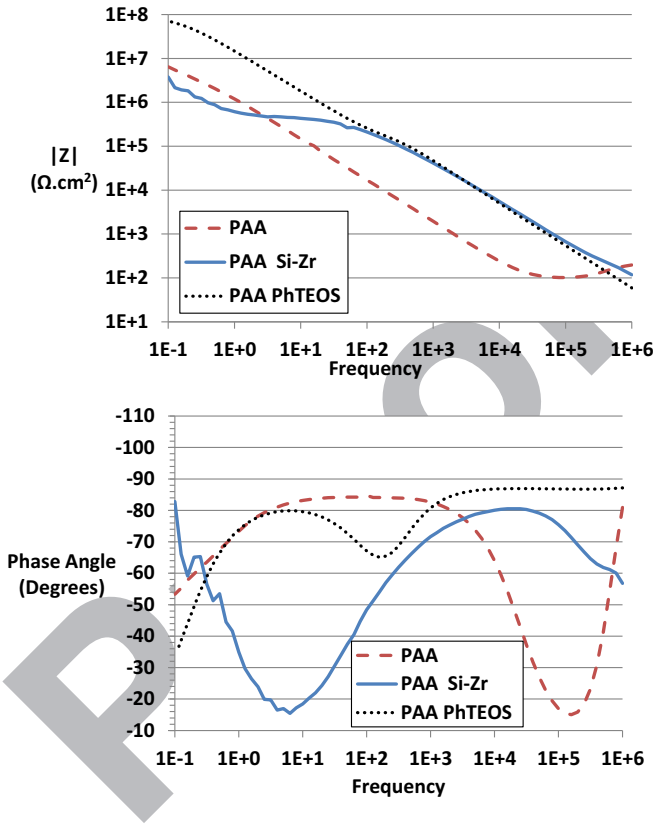

Figure 6. Impedance (top) and phase plot (bottom) for PAA sealed samples.

this sealer penetrates the porous network and the EIS response is as a result of the sol-gel/oxide composite layer. PhTEOS sol-gel sealed SAA anodic layers have been previously reported on 3003 and have produced a similar single time constant response.[26]

In contrast the SAA Si-Zr system exhibited a second time constant. As this sol-gel system acts as a surface coating on the anodic layer, the impedance response likely comprises the response from the surface coating and the barrier layer. The effect of the penetration of the PhTEOS sealer compared to the Si-Zr equivalent can be seen in the low frequency impedance values (<1 Hz). The PhTEOS system displayes higher impedance values, in this frequency region, due to the presence of the sol-gel in the pores.

The impedance and phase shift spectra for PAA sealed anodic layers can be in Figure 6. The sol-gel sealers showed an increase in impedance, compared to the PAA blank, in the high frequency range ($\sim 1 \times 10^4$ Hz). As the pores of PAA anodic layers are known to remain open indefinitely[1] the encapsulation of the sol-gel sealers results in this increase in the impedance compared to the PAA blank. In contrast to the SAA PhTEOS layer the PAA PhTEOS layer exhibits a two time constant response. The barrier layer of the PAA anodic layer will be thicker, due to higher forming voltage than the SAA equivalent, and perhaps this increased oxide thickness results in the discrimination between the sol-gel material and the anodic alumina barrier layer. The low frequency impedance of the PAA Si-Zr layer exhibits lower impedance values than the PhTEOS equivalent. The low frequency impedance (0.1 Hz) of the PAA Si-Zr is equivalent to the PAA blank. The PhTEOS sealer shows higher impedance than both the PAA blank and the PAA Si-Zr sample. This may be due to better penetration of the PhTEOS sol-gel to the base of the pores to the barrier layer.

The impedance and phase shift spectra for DA sealed anodic layers can be seen in Figure 7. The DA HTS samples exhibits a smilar response to the SAA HTS sample with a single time constant detected. Significantly, despite the increased thickness of the SAA layer compared to the sulphuric acid formed layer in the DA structure the impedance response are relatively similar. The EIS response in both

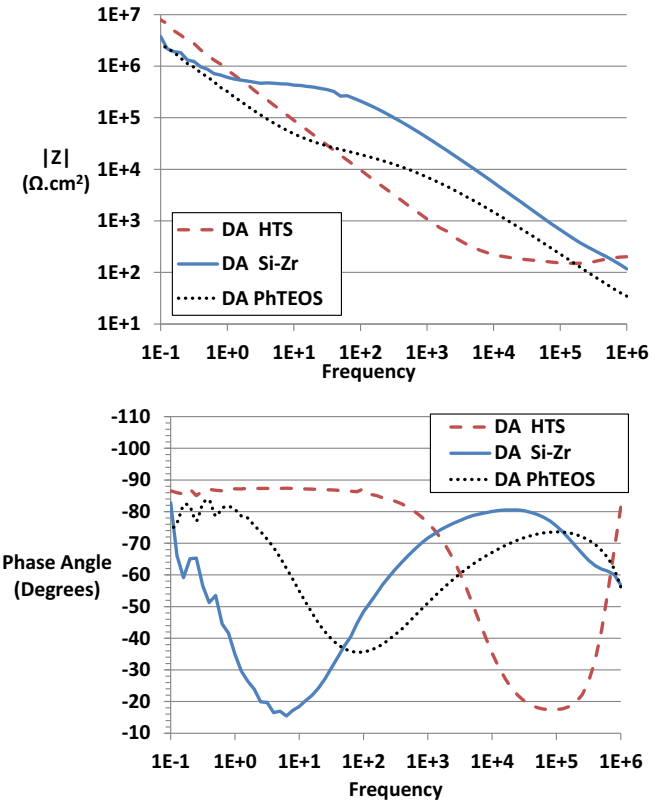

Figure 7. Impedance (top) and phase plot (bottom) for DA sealed samples.

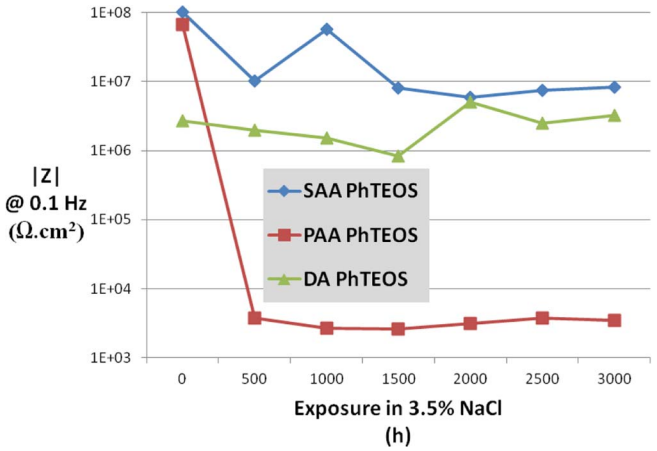

Figure 8. Plot of impedance as a function of time for PhTEOS treated layers exposed to 3.5% NaCl.

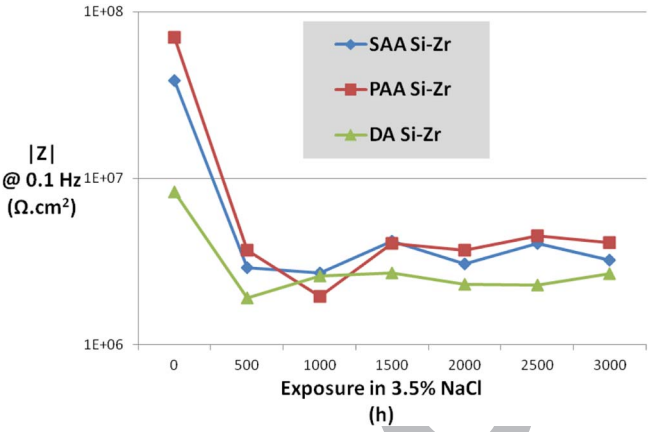

Figure 9. Plot of impedance as a function of time for Si-Zr treated layers exposed to 3.5% NaCl.

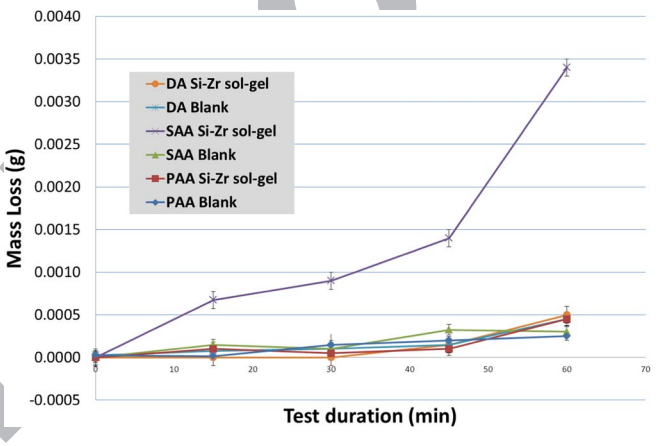

Figure 10. Rain erosion performance of anodised and sol-gel sealed systems on clad 2024-T3.

cases is from the barrier layer only.[37] For both of the sol-gel sealers the low frequency impedance (0.1 Hz) is lower than the DA HTS. This indicates, as expected, that the sealing effect has not progressed into the nanoporous structure and influenced the barrier layer properties. The presence of the sol-gel sealers may also have prevented any natural hydration which proceeds after the hydrothermal treatment as the sol-gels area applied almost immediately after hydrothermal sealing. This may explain the elevated low frequency impedance levels of the DA HTS compared to the sol-gel sealed equivalents. In the mid to high frequency range (>100 Hz) the sol-gel sealers show elevated impedance levels, compared to the DA HTS sample. The first time constant for the sol-gel sealers, appearing in the high frequency end of the spectrum, is as a result the sol-gel/oxide composite layer formed on the surface of the sample. The second time constant is the barrier layer contribution.

By plotting the impedance at 0.1 Hz over time the evolution of barrier properties can be determined for each sol-gel sealer. The protection properties of the PhTEOS sealed anodic layers during continuous exposure to the 3.5% NaCl solution can be seen in Figure 8. For the PhTEOS sealed anodic layers the SAA and DA layers appear relatively stable with a small gradual decrease up to 1500 h. The impedance of the PAA layer drops rapidly between 0 and 500 hr exposure. At this exposure time the PAA PhTEOS sealed layer exhibits extensive pitting and corrosion. The increased impedance of the SAA system compared to the DA is likely due to the longer anodising duration of the SAA system. Interestingly at 1500–2000 h both the SAA and DA PhTEOS sealed surfaces begin to increase marginally in impedance. The rapid deterioration of the PAA layer, despite achieving full encapsulation indicates the importance of the presence of an anodic layer that has the ability to seal naturally.

Again the evolution of the Si-Zr sealed anodic layers can be seen by plotting the low frequency impedance over exposure duration as seen in Figure 9. The Si-Zr sol-gel sealed anodic layers all experience an impedance drop of approximately one order of magnitude after 500 h. This initial drop is possibly due to uptake of electrolyte by the sol-gel coating. After this time the impedance of all the surfaces stabilise and remain consistent up to 3000 h exposure with no pitting or corrosion evident on the surfaces.

With the exception of the PhTEOS sealed PAA layer the anodised AA2024 surfaces appear stable up to 3000 h exposure. This is a significant duration for immersion in a chloride rich solution without a considerable loss in barrier properties.

Neutral salt spray.—Neutral salt spray exposure was also conducted on the anodised and sol-gel sealed samples and a corrosion rating has been assigned as per Table I. Unsealed equivalents have

Table I. Neutral salt spray corrosion ratings of anodic layers on AA2024-T3.

Treatment			NSS Duration							
Anodising	*Sol-gel*	First Cor $TCorr_0$	24 h	168 h	500 h	750 h	1000 h	1500 h	2000 h	3500 h
SAA	BLANK	24	1	6	50	50	-	-	-	-
PAA	BLANK	24	200	-	-	-	-	-	-	-
DA	BLANK	72	0	12	200	-	-	-	-	-
SAA	PhTEOS	24	1	12	50	100	-	-	-	-
PAA	PhTEOS	24	50	200	-	-	-	-	-	-
DA	PhTEOS	500	0	0	1	12	12	25	-	-
SAA	Si-Zr	3500	0	0	0	0	0	0	0	1
PAA	Si-Zr	500	0	0	1	12	25	200	-	-
DA	Si-Zr	1000	0	0	0	0	1	6	-	-

been used for comparison. As expected in the unsealed form, the SAA, PAA and DA surfaces offer little protection with corrosion occurring rapidly. The SAA and PAA layers exhibited pitting corrosion after 24 h exposure with the DA surface remaining clear of corrosion until 72 h exposure. Upon the onset of initial corrosion, pitting increases rapidly for all of the unsealed anodised surfaces. The presence of the sol-gel within the pores of the SAA layer appears to have a negative effect on corrosion prevention with a marginally higher level of pitting exhibited on the PhTEOS treated surface when compared to the unsealed SAA. This is possibly due to the effect on hydration due to the presence of the sol-gel within the aluminum oxide network. The sol-gel may retards the hydration of the surfaces as has been previously reported.[9] In the case of the PhTEOS PAA layer there is a marginal reduction in pitting however the improvement over the unsealed PAA is negligible. The PhTEOS sealed DA layer exhibited a marked increase in pitting prevention over the other PhTEOS sealed anodised finishes. This displays the value in utilising the DA process, as the natural hydration properties of the anodic layers are retained, while the sol-gel is also encapsulated in aluminum oxide.

The negative effect of the PhTEOS sealer on the SAA layer during neutral salt spray was not identified by the EIS analysis. One possible explanation is the difference in exposure area during the test. The much larger surface area exposed during the NSS test may be more indicative of the actual corrosion resistance than the smaller area EIS. For all samples the discrimination in corrosion resistance is greater by NSS than EIS indicating that the NSS is possibly a more aggressive test. The authors also believe that the EIS immersion cycle allows the natural hydration of the layers to proceed better than the salt fog test. Additionally, the salt fog test has reported to delaminate and remove sol-gel coatings attached to anodic layers,[27] which may result in a more aggressive corrosion effect.

The Si-Zr sol-gel displays enhanced pitting corrosion protection over the PhTEOS sol-gel sealed systems. The increased barrier properties as well as the inclusion of an active corrosion inhibitor results in a significant level of protection for all anodising treatments. The SAA layer in particular exhibits remarkable corrosion resistance with no evidence of pitting at 3500 h. The absence of pore penetration of the Si-Zr sol ensures that the natural hydration properties of the SAA layer are retained unlike the PhTEOS equivalent. Furthermore, the inclusion of an the tetrazine based corrosion inhibitor may also have a positive effect on the integrity of the SAA layer as tetrazines are known to bind to and chelate copper ions.[38] These inhibitors have been studied as standalone treatments for anodic layers and have shown increased ability to inhibit pitting corrosion.[38] The DA equivalent shows a higher degree of degradation, when compared to the SAA equivalent, possibly due to the decreased thickness of the SAA layer. The worst performing Si-Zr sealed layer is the PAA.

Rain erosion.—Anodising is often used to increase the surface hardness and abrasion resistance of aluminum alloys.[1] By incorporating the sol-gel coating into the aluminum oxide network elevated mechanical properties are afforded to the sol-gel coating. This will improve the hardness, abrasion resistance and impact resistance of the sol-gel coatings. A significant advantage of increased mechanical performance for the aerospace industry is the decreased effect of rain erosion. Erosion of aerospace grade aluminum alloys by impinging water droplets is a significant issue especially during aircraft take-off and landing.[39,40]

Whirling arm rain erosion evaluation of the Si-Zr sol-gel sealed clad 2024-T3 samples was conducted and the weight loss over the 60 min exposure was recorded as seen in Figure 9. The weight loss for the sol-gel applied on the SAA is significantly greater than any other surface tested. From the EDX analysis (Figure 4), it is determined that the sol-gel forms a surface coating on the SAA surface with limited encapsulation in the porous anodic alumina. Therefore, the rain erosion and weight loss of this system is of the sol-gel coating only, which is mechanically inferior to the aluminum oxides produced from SAA, PAA and DA as well as the sol-gel/alumina composites produced from sol-gel encapsulation.

This indicates that the encapsulation of the sol-gel coatings in anodic alumina presents a significant improvement in rain erosion. The weight loss of the bare anodic layers or sol-gel encapsulated layers is minimal.

Sol-gel materials have been studied extensively for replacement of chromate materials as they can act as reservoirs for active corrosion inhibitors. However for many sol-gel coating additives there is a critical concentration after which the additive affects the film forming properties and integrity of the applied sol-gel film. Excess amounts of corrosion inhibitors have shown to have a negative effect on film forming properties of sol-gel coatings.[41–43] By utilising a duplex anodic oxide, the active corrosion inhibitors can be incorporated in the SAA layer at a significantly higher concentration while the sol-gel can be encapsulated in the porous PAA network. As shown from the results, the DA layer is particularly suitable for sol-gel sealing. Due to the low thickness of sol-gel coatings, the PAA layer can be tailored to result in full encapsulation of the sol-gel coating within the anodic structure. Furthermore, conventional sealing methods can be applied to the SAA base layer of the DA structure. This results in elevated corrosion resistance while also preventing the sol-gel material from migrating into the SAA pores. This becomes particularly important with clad AA2024 or non copper containing alloys as the natural hydration properties of SAA layer is therefore not affected by the presence of the sol-gel material. The DA process developed can also be utilised for adhesion and bonding applications while also retaining a significant level of corrosion resistance on aluminum alloys.

Conclusions

Duplex anodic layers have been developed to achieve sol-gel encapsulation in porous anodic alumina to ensure that the natural hydration properties of anodised aluminum is retained. By encapsulating sol-gel materials in phosphoric acid anodised aluminum the mechanical properties of the sol-gel coatings are enhanced. By forming a sulphuric acid anodised layer between the sol-gel/oxide composite and the substrate the combined corrosion resistance is significantly enhanced. The value of utilising the duplex anodic layers is evident due to the achievable anti-corrosion performance on corrosion prone 2024-T3, sealed with a simple organically modified silane based sol-gel. The performance is further enhanced by applying a Si-Zr hybrid sol-gel with active tetrazine based inhibitor. For all systems the absence of the sol-gel from the pores of the SAA layers is critical to allow the natural or accelerated hydration of the systems to proceed.

Acknowledgments

This work is supported by Enterprise Ireland under the Technology Gateway Programme and the European Union under the Seventh Framework Programme, project 266029 “Aeromuco”.

References

1. S. Wernick, R. Pinner, and P. G. Sheasby, *The Surface Treatment and Finishing of Aluminum and its Alloys*, 5th ed., Finishing Publications Ltd.1987.
2. V. F. Henley, *Anodic Oxidation of Aluminium & its Alloys*, Pergamon Press 1982.
3. S. J. Garcia-Vergara, L. Iglesias-Rubianes, C. E. Blanco-Pinzon, P. Skeldon, G. E. Thompson, and P. Campestrini, “Mechanical instability and pore generation in anodic alumina,” *Proceedings of the Royal Society A: Mathematical, Physical and Engineering Science*, **462**, 2345 (2006).
4. S. J. Garcia-Vergara, P. Skeldon, G. E. Thompson, and H. Habazaki, “Stress generated porosity in anodic alumina formed in sulphuric acid electrolyte,” *Corrosion Science*, **49**, 3772 (2007).
5. S. J. Garcia-Vergara, P. Skeldon, G. E. Thompson, T. Hashimoto, and H. Habazaki, “Compositional Evidence for Flow in Anodic Films on Aluminum under High Electric Fields,” *Journal of The Electrochemical Society*, **154**, C540 (2007).
6. S. J. Garcia-Vergara, P. Skeldon, G. E. Thompson, and H. Habakaki, “Tracer studies of anodic films formed on aluminum in malonic and oxalic acids,” *Applied Surface Science*, **254**, 1534 (2007).
7. J. A. González, M. Morcillo, E. Escudero, V. López, and E. Otero, “Atmospheric corrosion of bare and anodized aluminum in a wide range of environmental conditions. Part I: Visual observations and gravimetric results,” *Surf. Coat. Technol.*, **153**, 225 (2002).

8. J. A. Gonzalez, M. Morcillo, E. Escudero, V. Lopez, A. Bautista, and E. Otero, Self-sealing of unsealed aluminum anodic oxide films in very different atmospheres, Revista de Metalurgia, Extr CODEN RMTGAC (2003) 110.
9. M. Whelan, J. Cassidy, and B. Duffy, "Sol–gel sealing characteristics for corrosion resistance of anodised aluminum," *Surf. Coat. Technol.*, **235**, 86 (2013).
10. M. J. Bartolomé, J. F. del Río, E. Escudero, S. Feliu Jr, V. López, E. Otero, and J. A. González, "Behaviour of different bare and anodised aluminum alloys in the atmosphere," *Surf. Coat. Technol.*, **202**, 2783 (2008).
11. E. Escudero, V. López, E. Otero, M. J. Bartolomé, and J. A. González, "Behaviour of anodised aluminum in very long-term atmospheric exposure," *Surf. Coat. Technol.*, **201**, 7303 (2007).
12. T. Hashimoto, X. Zhou, P. Skeldon, and G. E. Thompson, "Structure of the Copper–Enriched Layer Introduced by Anodic Oxidation of Copper-Containing Aluminium Alloy," *Electrochim. Acta*, **179** 394.
13. L. Domingues, J. C. S. Fernandes, M. Da Cunha Belo, M. G. S. Ferreira, and L. Guerra-Rosa, "Anodising of Al 2024-T3 in a modified sulphuric acid/boric acid bath for aeronautical applications," *Corros. Sci.*, **45**, 149 (2003).
14. M. A. Arenas, A. Conde, and J. J. de Damborenea, "Effect of acid traces on hydrothermal sealing of anodising layers on 2024 aluminum alloy," *Electrochim. Acta*, **55**, 8704 (2010).
15. P. C. R. Varma, J. Colreavy, J. Cassidy, M. Oubaha, B. Duffy, and C. McDonagh, "Effect of organic chelates on the performance of hybrid sol–gel coated AA 2024-T3 aluminum alloys," *Prog. Org. Coat.*, **66**, 406 (2009).
16. P. C. R. Varma, P. Periyat, M. Oubaha, C. McDonagh, and B. Duffy, "Application of niobium enriched ormosils as thermally stable coatings for aerospace aluminum alloys," *Surf. Coat. Technol.*, **205**, 3992 (2011).
17. R. V. Padinchare Covilakath, J. Cassidy, M. Oubaha, C. McDonagh, J. Colreavy, and B. Duffy, "Corrosion Protection Properties of Various Ligand Modified Organic Inorganic Hybrid Coating on AA 2024-T3," *ECS Transactions*, **24**, 231 (2010).
18. J. Livage, M. Henry, and C. Sanchez, "Sol-gel chemistry of transition metal oxides," *Progress in Solid State Chemistry*, **18**, 259 (1988).
19. G. S. C. J. Brinker, *Sol-Gel Science: The Physics and Chemistry of Sol-Gel Processing*, Academic Press, San Diego, CA, 1990.
20. L. L. Hench and J. K. West, "The sol-gel process," *Chemical Reviews*, **90**, 33 (1990).
21. M. L. Zheludkevich, I. M. Salvado, and M. G. S. Ferreira, "Sol-gel coatings for corrosion protection of metals," *Journal of Materials Chemistry*, **15**, 5099 (2005).
22. M. Guglielmi, "Sol-gel coatings on metals," *Journal of Sol-Gel Science and Technology*, **8**, 443 (1997).
23. C. Sanchez, B. Julian, P. Belleville, and M. Popall, "Applications of hybrid organic-inorganic nanocomposites," *Journal of Materials Chemistry*, **15**, 3559 (2005).
24. P. G.-R. C. Sanchez and Functional Hybrid Materials 2004.
25. R. L. Parkhill, E. T. Knobbe, and M. S. Donley, "Application and evaluation of environmentally compliant spray-coated ormosil films as corrosion resistant treatments for aluminum 2024-T3," *Progress in Organic Coatings*, **41**, 261 (2001).
26. M. Whelan, J. Cassidy, and B. Duffy, "Sol-gel Sealing Characteristics for Corrosion Resistance of Anodised Aluminium," *Surface and Coatings Technology* (2013), doi: 10.1016/j.surfcoat.2013.07.018.
27. V. R. Capelossi, M. Poelman, I. Recloux, R. P. B. Hernandez, H. G. de Melo, and M. G. Olivier, "Corrosion protection of clad 2024 aluminum alloy anodized in tartaric-sulfuric acid bath and protected with hybrid sol–gel coating," *Electrochim. Acta*, **124**, 69 (2014).
28. G. W. Critchlow, K. A. Yendall, T. Cartwright, and I. A. Ashcroft, "Environmentally-friendly surface treatments, Automotive Adhesives, Sealants & Coatings," *Proceedings of the Conference*, Rapra Smithers, Stuttgart, Germany, 2008, pp. 18/11-18/11.
29. J. Colreavy, B. Duffy, P. C. R. Varma, H. Hayden, and O. Mohamed, Sol-Gel Coating Compositions and their Process of Preparation, EP2220176 (2010).
30. M. García-Rubio, M. P. de Lara, P. Ocón, S. Diekhoff, M. Beneke, A. Lavía, and I. García, "Effect of postreatment on the corrosion behaviour of tartaric sulphuric anodic films," *Electrochim. Acta*, **54**, 4789 (2009).
31. V. Moutarlier, M. P. Gigandet, J. Pagetti, and L. Ricq, "Molybdate/sulfuric acid anodising of 2024-aluminum alloy: influence of inhibitor concentration on film growth and on corrosion resistance," *Surf. Coat. Technol.*, **173**, 87 (2003).
32. O. Zubillaga, F. J. Cano, I. Azkarate, I. S. Molchan, G. E. Thompson, and P. Skeldon, "Synthesis of anodic films in the presence of aniline and TiO2 nanoparticles on AA2024-T3 aluminum alloy," *Thin Solid Films*, **517**, 6742 (2009).
33. M. García-Rubio, P. Ocón, M. Curioni, G. E. Thompson, P. Skeldon, A. Lavía, and I. García, "Degradation of the corrosion resistance of anodic oxide films through immersion in the anodising electrolyte," *Corros. Sci.*, **52**, 2219 (2010).
34. K. Shimizu, H. Habazaki, P. Skeldon, G. E. Thompson, and G. C. Wood, "Migration of oxalate ions in anodic alumina," *Electrochim. Acta*, **46**, 4379 (2001).
35. K. Shimizu, H. Habazaki, P. Skeldon, G. E. Thompson, and G. C. Wood, "Migration of sulfate ions in anodic alumina," *Electrochim. Acta*, **45**, 1805 (2000).
36. A. Santos, L. Vojkuvka, J. Pallarés, J. Ferré-Borrull, and L. F. Marsal, "In situ electrochemical dissolution of the oxide barrier layer of porous anodic alumina fabricated by hard anodization," *J. Electroanal. Chem.*, **632**, 139 (2009).
37. M. Franco, S. Anoop, R. Uma Rani, and A. K. Sharma, Porous Layer Characterization of Anodized and Black-Anodized Aluminium by Electrochemical Studies, ISRN Corrosion, 2012 Article ID 323676 (2012) 12.
38. M. Whelan, K. Barton, J. Cassidy, J. Colreavy, and B. Duffy, "Corrosion inhibitors for anodised aluminum," *Surf. Coat. Technol.*, **227**, 75 (2013).
39. P. Lammel, L. D. Rafailovic, M. Kolb, K. Pohl, A. H. Whitehead, G. Grundmeier, and B. Gollas, "Analysis of rain erosion resistance of electroplated nickel–tungsten alloy coatings," *Surf. Coat. Technol.*, **206**, 2545 (2012).
40. E. F. Tobin, T. M. Young, D. Raps, and O. Rohr, "Comparison of liquid impingement results from whirling arm and water-jet rain erosion test facilities," *Wear*, **271**, 2625 (2011).
41. P. C. R. Varma, B. Duffy, and J. Cassidy, "Influence of magnesium nitrate on the corrosion performance of sol–gel coated AA2024-T3 aluminum alloy," *Surf. Coat. Technol.*, **204**, 277 (2009).
42. J. H. Osborne, K. Y. Blohowiak, S. R. Taylor, C. Hunter, G. Bierwagon, B. Carlson, D. Bernard, and M. S. Donley, "Testing and evaluation of nonchromated coating systems for aerospace applications," *Prog. Org. Coat.*, **41**, 217 (2001).
43. M. Schem, T. Schmidt, J. Gerwann, M. Wittmar, M. Veith, G. E. Thompson, I. S. Molchan, T. Hashimoto, P. Skeldon, A. R. Phani, S. Santucci, and M. L. Zheludkevich, "CeO2-filled sol–gel coatings for corrosion protection of AA2024-T3 aluminum alloy," *Corros. Sci.*, **51**, 2304 (2009).

Q2

Queries

Q1: AU: Please provide text citation for Fig. 10.

Q2: AU: Please provide a digital object identifier (doi) for Ref(s) 22. For additional information on doi's please select this link: http://www.doi.org/. If a doi is not available, no other information is needed from you.